Assessment of surface energetic heterogeneity of synthetic Na-saponites. The role of layer charge

L. J. MICHOT* AND F. VILLIÉRAS

Laboratoire Environnement et Minéralurgie, INPL-ENSG-CNRS UMR 7569, BP 40, 54501 Vanduvre Cedex, France

ABSTRACT: High-resolution gas adsorption techniques were used to analyse the evolution of the aspect ratio and adsorption energy distribution on synthetic saponite samples with increasing layer charge. Using Ar as a gaseous probe, the aspect ratio of the saponite particles can be determined easily by decomposing the derivative adsorption isotherms and taking into account high-energy sites which can be assigned to talc-like ditrigonal cavities. Changes in the shape of the elementary particles are observed for layer charges above 1.30, i.e. when all the ditrigonal cavities contain at least one Al atom substituting for Si. When N_2 is used as a probe, high-energy sites that could be wrongly interpreted as micropores on the basis of classical t-plot treatments are observed whatever the layer charge. Using the information obtained from both Ar and N_2, schemes for describing adsorption can be proposed for all layer charges and suggest complex adsorption mechanisms for charged clay minerals.

Phyllosilicates play an important role in natural and industrial processes because, due to their important specific surface areas, they can exchange organic and inorganic molecules at solid-liquid or solid-gas interfaces. To understand the mechanisms involved, the surface properties of phyllosilicates have to be determined precisely. For surface exchange purposes, phyllosilicates can be considered as heterogeneous minerals as they present at least two different types of surfaces, basal and broken-edge faces, with different surface chemistry and properties. This is very well illustrated in the case of kaolinite, the reactive surfaces of which are mainly located on the edge faces. This predominance of edge faces was evidenced in numerous studies dealing with adsorption at solid-liquid interfaces (Conley & Lloyd, 1971; Cases *et al.*,

1986; Kronberg *et al.*, 1986; Braggs *et al.*, 1994; Brady *et al.*, 1996; Ward & Brady, 1998). In the case of illite, many studies have shown that cation adsorption occurs on both basal and lateral surfaces (Du *et al.*, 1997; Kulik *et al.*, 2000). Similar conclusions have been reported by Sondi *et al.* (1997) for chlorite.

Therefore, particle shape is a very important feature of clay minerals which depends on the physicochemical conditions of crystallization, growth, transport and deposition. This has been well established for kaolinites (Cases *et al.*, 1986; Giese 1988; Psyrillos *et al.*, 1999) where a close relationship exists between crystallinity, size and shape (Cases *et al.*, 1986). Well-crystallized kaolinites generally present clearly defined hexagonal shapes.

Several techniques have been proposed for determining the aspect ratio of platy clay minerals. Assuming that the coherent scattering length is equal to the clay particle thickness, an average

* E-mail: laurent.michot@ensg.inpl-nancy.fr

thickness can be derived from X-ray diffraction (XRD) analysis by exploiting the shape of basal reflections (Srodoń & Elsass, 1994; Šucha *et al.*, 1996; Sánchez-Soto *et al.*, 1997). More sophisticated treatments take into account different particle-size distributions using, for instance, the MudMaster software developed by Eberl and colleagues (Eberl *et al.*, 1996; Sánchez-Soto *et al.*, 1997). Methods based on particle-size distribution measurements can also be used to derive particle thickness and length (Liétard *et al.*, 1980; Cases *et al.*, 1986; Mühlenweg & Dan Hirleman, 1998; Ma & Eggleton, 1999). These methods are generally rapid but the data should be considered with caution because of possible artefacts in the determination of particle-size distributions (Cases *et al.*, 1986).

Scanning electron microscopy (SEM), transmission electron microscopy (TEM), and atomic force microscopy (AFM) image analysis have also been used to study the shape and size of various clay minerals (Thompson *et al.*, 1981; Cases *et al.*, 1986; Šucha *et al.*, 1996; Kuwahara *et al.*, 1998; Zbik & Smart, 1998, 1999). When performed carefully, these techniques allow near-reality visualization of clay particles. The TEM and AFM analyses are particularly suitable for studying growth steps on basal faces (Thompson *et al.*, 1981; Nagy & Blum, 1994; Kuwahara *et al.*, 1998; Zhang & Bailey, 1998; Zbik & Smart, 1998). However, the determination of mean values requires careful sample preparation and the analysis of a large number of images (Cases *et al.*, 1986; Zbik & Smart, 1999).

A different approach to shape determination is to use molecular probe adsorption techniques, at either solid-liquid (Conley & Lloyd, 1971; Cases *et al.*, 1986; Poirier & Cases, 1991) or solid-gas interfaces (Cases *et al.*, 1986; Michot *et al.*, 1993, 1994; Villiéras *et al.*, 1992, 1997a,b; Bardot, 1998; Bardot *et al.*, 1998, 2000). These methods are based on the fact that the chemical nature of edge and basal faces is different, which changes their interaction with adsorbing molecules. At the gas-solid interface, using Ar as a molecular probe, reliable values of aspect ratios could be obtained for uncharged clay minerals such as talc and kaolin (Cases *et al.*, 1986; Michot *et al.*, 1993, 1994; Villiéras *et al.*, 1992, 1997a,b). The situation is a little more complex for charged clay minerals (e.g. illite) as the nature of the compensating surface cation influences the shape of the adsorption isotherms (Bardot 1998; Bardot *et al.*, 1998, 2000). Except in the case of talc, N_2 cannot be used for shape determination as, due to its inducible quadrupolar momentum, it shares specific interactions with sites on both basal and lateral faces, which prevents unequivocal assignments of isotherm features.

The aim of the present paper is to study Ar and N_2 adsorption on a series of synthetic Na-saponite samples. The nature of the compensating cation being fixed, the influence of layer charge can be analysed in detail, talc representing the non-charged end-member of such series.

EXPERIMENTAL

Synthesis

Synthetic saponites were prepared at the Centre de Recherches sur la Synthèse et la Chimie des Minéraux (Orléans, France) by hydrothermal synthesis at $400°C$ under 1 kbar water pressure, with run durations of 4 weeks, in Morey-type externally heated pressure vessels. The samples were insulated from the vessel wall by a silver coating. The starting products were gels of appropriate compositions, prepared by coprecipitation of Na, Mg, Al and Si hydroxides at pH = 14, according to the gelling method of Hamilton & Henderson (1968). The source of Na was Na_2CO_3; the sources of Al and Mg were titrated solutions of their nitrates; and the source of Si was $(C_2H_5O)_4Si$ (TEOS). Prior to hydrothermal synthesis, the starting product was dried and calcined, and then crushed for further homogenization. After hydrothermal synthesis, the sample was quenched and examined by XRD and ^{29}Si and ^{27}Al nuclear magnetic resonance (NMR) to confirm the single phase character (Lambert *et al.*, 1994). The resulting structural formula is: $Na_x(Si_{8-x}Al_x)(Mg_6)O_{20}(OH)_4$, with $0.7 \leqslant x \leqslant 2.0$. The samples will be referred to as SNa-*x*, where *x* is the negative layer charge, per unit cell.

METHODS

CEC measurements

The cationic exchange capacities (CEC) of the samples were determined by exchanging the cations with the hexa-aminecobalt (II) ion $[Co(NH_3)_6]^{3+}$ (Rémy & Orsini, 1976). Clay samples of 500 mg were dispersed in 30 ml of a 0.05 M cobaltihex-

amine solution. The suspension was stirred for 2 h and centrifuged twice. The equilibrium concentration of the supernatant in cobaltihexamine was determined colorimetrically (Co absorption band at 473 nm) on a UV-visible spectrometer (Shimadzu UV 2100) that yields the CEC.

X-ray diffraction

The XRD patterns were obtained on powdered samples by using a Jobin-Yvon diffractometer working using Cu-$K\alpha_1$ radiation. The d_{001} spacings were measured at the 001 line maximum.

Ar and N₂ adsorption

Classical N_2 adsorption-desorption isotherms were obtained at 77 K on a lab-built automatic volumetric adsorption apparatus. The experimental conditions were a sample mass of ~1 g, outgassing under a residual pressure of 0.01 Pa at 150°C. Surface areas were determined using the BET treatment. The presence of micropores in the samples was assessed using the t-plot method (De Boer *et al.,* 1966).

High-resolution low-pressure isotherms of Ar and N_2 were recorded on a lab-built automatic quasi-equilibrium volumetric set-up (Michot *et al.,* 1990; Villiéras *et al.,* 1992). In this method, a slow, constant and continuous flow of adsorbate was introduced into the adsorption cell. From the recording of quasi-equilibrium pressures *vs.* time, the adsorption isotherms were derived. The experimental conditions were a sample mass of ~1 g, outgassing at 0.001 Pa at a temperature of 150°C. The data were then treated using the improved Derivative Isotherm Summation (DIS) procedure designed by Villiéras *et al.* (1992, 1997a) to examine the surface energetic heterogeneity of the samples. Due to the large number of experimental data points acquired by the quasi-equilibrium procedure, the experimental derivative of the adsorbed quantity as a function of the logarithm of relative pressure can be calculated accurately. The total derivative adsorption isotherm on a heterogeneous surface is simulated by the sum of local theoretical derivative adsorption isotherms on heterogeneous surfaces with random heterogeneity.

The adsorption isotherm on a heterogeneous surface formed with different energetic domains can be written as:

$$\theta_t = \sum_i X_i \theta_{it} = \sum_i X_i \int_\Omega \theta_i(\varepsilon) \cdot \chi_i(\varepsilon) \cdot d\varepsilon \quad (1)$$

Where θ_t is the total adsorption isotherm, θ_{it}, the adsorption isotherms on the different energetic domains of the surface, X_i is its contribution to θ_t, ε is the adsorption energy, Ω is the physical domain of ε, $\theta_i(\varepsilon)$ a 'local' theoretical adsorption isotherm and $\chi_i(\varepsilon)$ the dispersion of ε on the ith domain. The theoretical isotherms used (Villiéras *et al.,* 1997a) are obtained by first approximating the energy distribution by the condensation approximation (CA). For describing adsorption into micropores, a generalization of the Dubinin-Asthakov isotherm was proposed:

$$\theta_{it}(P/P_0) = e^{-\left[\frac{kT}{E_i}\ln\left(\frac{P_i^0}{P}\right)\right]^{r_i}} \quad (2)$$

where E_i is the variance of $\chi_i(\varepsilon)$ and r_i a parameter governing the shape of the distribution function. For $r_i = 2$, equation 2 becomes the Dubinin-Radushkevich isotherm. Equation 2 can be extended to take into account the effect of lateral interactions ω by replacing

$$\frac{kT}{E}\ln\left(\frac{P^0}{P}\right)$$

by

$$\Delta = \frac{kT}{E}\ln\left(\frac{P^0}{P}\right) - \frac{\omega\theta}{E}$$

The derivative of equation 2 with regard to the logarithm of the pressure is:

$$\left[\frac{\partial\theta_t}{\partial\ln P}\right]_T = \frac{r\frac{kT}{E}[\Delta]^{r-1}\theta}{\left(1 - \frac{r\omega}{E}[\Delta]^{r-1}\theta\right)} \quad (3)$$

It is a Gaussian-like function widened on the low-energy side for $r_i < 3$ and widened on the high-energy side for $r_i > 3$.

The expression of the second derivative is relatively complicated and is obtained through a numerical procedure. In the DIS method, the identification of the different parameters is obtained from the coordinates of the maximum and from the width of the derivative. The mathematical relations between E_i, r_i and P_i^0 can be derived easily from the expression of the first and second derivatives of equation 2 when the second derivative equals zero.

Then, for given values of r and P^0, the amount adsorbed on the domain i, X_i, can be obtained from the comparison between the height of the experimental and calculated maxima at P^*:

$$X_i = \frac{dV_{ads}/d\ln(P^*/P_0)}{d\theta_i/d\ln(P^*/P_0)} \quad (4)$$

In practice, r_i and P_i^0 are fixed and, from the position of a maximum P^*, the adsorption capacity X_i and E_i are calculated. r_i and P_i^0 are adjusted until the simulated curve matches the experimental one.

A multilayer extension of equation 2 has also been proposed (Villiéras et al., 1997a). From this model, it is possible to extract the contribution of the first adsorbed layer. The multilayer adsorption isotherm gives us:

$$\theta_{it}(P_a) = (1 + P_a)\theta_{i1}(P_a) \quad (5)$$

where θ_{i1} corresponds to the adsorption of the first layer and is calculated using equation 3 with P_a defined as follows:

$$P_a = \frac{P/P_0}{1 - k'(P/P_0)} \quad (6)$$

where k' is generally chosen equal to 1. The first derivative leads to:

$$\left[\frac{\partial\theta_t}{\partial\ln P}\right] =$$

$$\left[\frac{(P_a + 1)^2 r\Delta^{r-1}\left(\frac{kT}{E}\right)}{1 - \left(\frac{\omega}{E}\right)r\Delta^{r-1}e^{-\Delta r}} + P_a(P_a + 1)\right]e^{-\Delta r} \quad (7)$$

where

$$\Delta = \frac{\varepsilon_c - \varepsilon^0}{E} = -\frac{kT}{E}\ln P_a - \frac{kT\ln K_r + \varepsilon^0}{E} - \frac{\omega}{E}\theta_{1t} \quad (8)$$

and

$$\Delta' = \left(\frac{\partial\Delta}{\partial\ln P}\right)_T = -\frac{kT}{E}(P_a + 1)-$$

$$\left(\frac{\omega}{E}\right)\frac{1}{P_a + 1}\left[\left[\frac{\partial\theta_t}{\partial\ln P}\right]_T - \theta_t P_a\right] \quad (9)$$

In this case, the experimental parameter corresponding to the different domains is obtained in the same way as from equation 3. In some cases, especially for low-energy adsorption domains, the maxima are not observed. If an inflection point can

be determined, the parameters are calculated from the inflection point properties in the same way as for a maximum. Finally, if no inflection point appears, i.e. if r_i is close to 1, all the parameters must be adjusted. This is accomplished by choosing a point on the derivative curve; parameters are adjusted step by step in order to calculate the derivative going through this point and properly matching the experimental curve.

RESULTS

Figure 1 displays the experimental CEC values as a function of theoretical layer charge (Thomas et al., 1999). The dotted line represents the values expected on the basis of the theoretical layer charge. There is a near perfect match between experimental and theoretical values for layer charges $\leqslant 1.60$. For higher charges, the experimental CECs are slightly lower than what would be expected from structural data. In fact, ^{27}Al MAS NMR measurements (Pelletier et al., submitted) showed that the samples with charges of 1.8 and 2.0 contained small amounts of octahedral Al and should then be considered as vermiculites rather than as true saponites. This trend is also noticeable in the evolution of the d_{001} values measured by XRD (Fig. 2). The highest-charge samples exhibit a
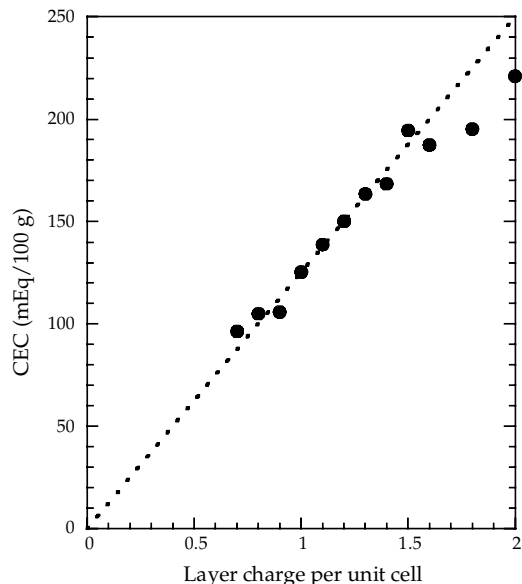

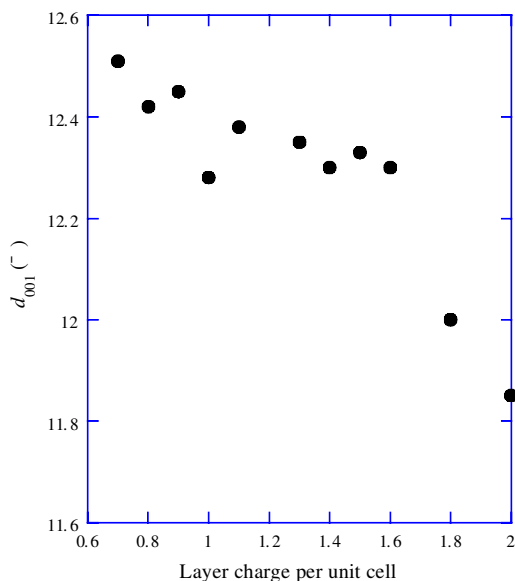FIG. 1. Evolution of the CEC of synthetic saponites with increasing layer charge.

FIG. 2. Evolution of the position of the d_{001} reflection of synthetic saponites with increasing layer charge.

lower *d*-spacing, ~11.9 Å, which is typical of Na-vermiculites (De la Calle & Suquet, 1988). For this reason, our analysis of the gas adsorption properties will only deal with samples with *x* values from 0.70 to 1.60.

Figure 3 displays the N_2 adsorption-desorption isotherms obtained on the different samples, whereas Table 1 shows the relevant parameters

deduced from the BET and t-plot treatments. All the synthetic saponite samples appear microporous with microporous volumes accounting for ~25% of the BET monolayer capacity. The origin and assessment of this microporosity will be discussed in detail in the following sections of this paper. The total surface area of the samples varies between 32 and 70 $m^2 g^{-1}$. The samples with the highest charges (1.40 to 1.60) present surface areas that are significantly lower. The variations in surface areas are not directly correlated to variations in the stacking order along the *c* direction as the half-width measured for both the 001 and 004 reflections do not vary strongly with the layer charge.

Figure 4 shows the derivative Ar adsorption isotherms of the ten saponite samples together with their decomposition obtained from the DIS procedure whereas Table 2 presents the parameters corresponding to the various domains obtained from the decomposition. The evolution of the derivative adsorption isotherms with increasing layer charges reveals the following trends: (1) A major peak (domain 3 in Table 2) is located at ln(*P/P*$_0$) values of approximately −4.9 k*T*. The position of this peak on the *x* axis is nearly constant with charge. On the other hand its width decreases regularly with increasing layer charge. This is illustrated by the r values used in the decomposition procedure which increase with layer charge. (2) A peak (domain 2 in Table 2) located at

TABLE 1. Parameters deduced from the use of the BET and t-plot treatment on the adsorption of N_2 at 77 K on synthetic saponites with increasing layer charge. Outgassing conditions: 150°C, 0.01 Pa.

Layer charge per unit cell	V_m[1] $(cm^3 g^{-1})$	C_{BET}	S_{BET} $(m^2 g^{-1})$	St_{or}[2] $(m^2 g^{-1})$	V_{mic}[3] $(cm^3 g^{-1})$	S_{ext}[4] $(m^2 g^{-1})$
0.7	13.83	400	60.4	64.8	3.5	49.5
0.8	10.53	519	46.0	50.2	3.2	35.2
0.9	10.17	583	44.4	48.3	2.7	35.6
1.0	15.04	411	65.7	70.7	3.4	54.3
1.1	12.29	414	53.7	58.2	2.6	45.8
1.2	13.82	485	60.4	65.0	3.5	48.5
1.3	10.04	226	43.9	46.1	2.3	35.6
1.4	6.89	344	30.1	32.1	1.7	24.2
1.5	7.73	409	33.8	35.7	1.7	28.4
1.6	8.16	399	35.6	37.1	2.0	28.4

[1] Monolayer capacity derived from the BET treatment
[2] Surface area derived from the slope of the straight line passing through the origin of the t-plot.
[3] Liquid microporous volume derived from the ordinate at the origin of the second straight line of the t-plot.
[4] Surface area derived from the slope of the second straight line of the t-plot
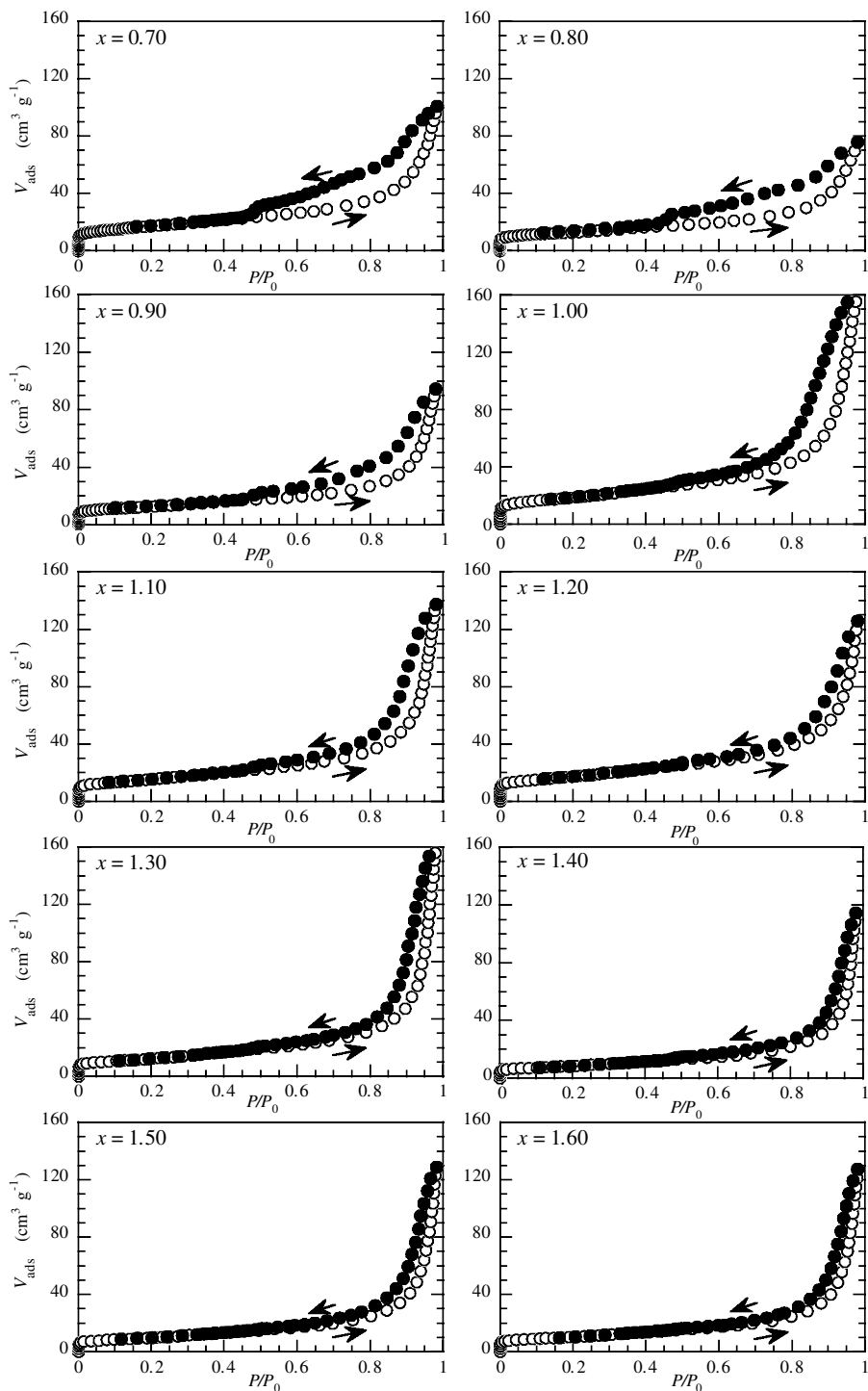
L. J. Michot and F. Villiéras

FIG. 3. Adsorption-desorption isotherms of N_2 at 77 K on synthetic saponites with increasing layer charge. Outgassing conditions: 150°C, 0.01 Pa.
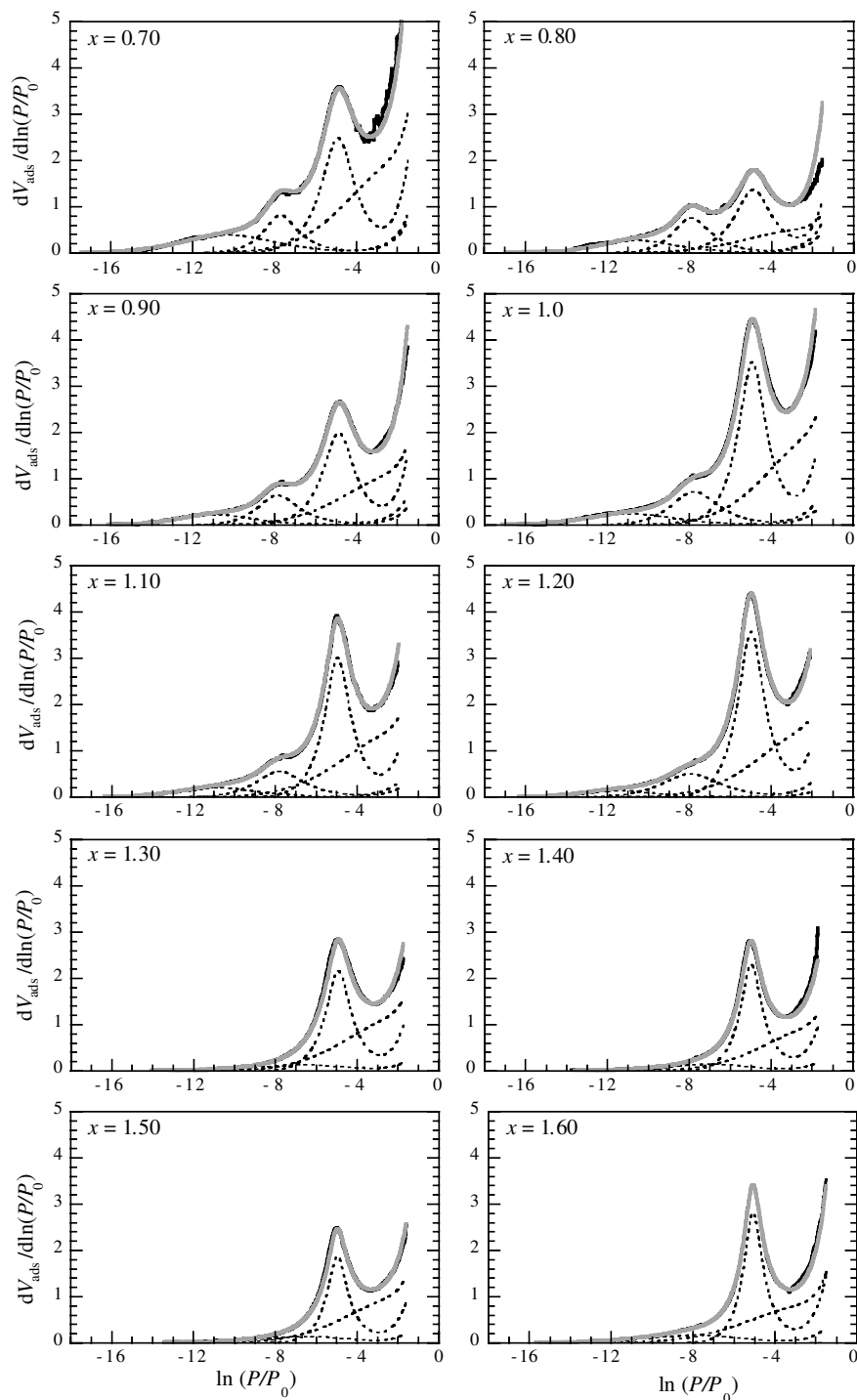
FIG. 4. Derivative Ar adsorption isotherms obtained at 77 K on synthetic saponites with increasing layer charge together with their decomposition using the Derivative Isotherm Summation (DIS) method. Outgassing conditions: 150°C, 0.001 Pa.

TABLE 2. Main parameters obtained from the application of the DIS method to Ar adsorption at 77 K on saponites with increasing layer charge. Outgassing conditions: 150°C, 0.001 Pa.

Layer charge per unit cell		0.70	0.80	0.90	1.00	1.10	1.20	1.30	1.40	1.50	1.60
Domain 1	$\ln(P/P_0)$	−10.30	−10.59	−10.96	−10.94	−10.68	−11.60	−	−	−	−
	V_m	2.30	1.34	1.09	1.36	1.03	0.67	−	−	−	−
	r	3.50	4.00	4.20	3.75	4.05	4.50	−	−	−	−
Domain 2	$\ln(P/P_0)$	−7.70	−7.92	−7.87	−7.78	−7.81	−7.95	−6.53	−6.97	−6.40	−7.85
	V_m	1.96	1.94	1.78	2.23	1.74	1.85	0.75	0.77	0.73	0.98
	r	4.10	4.30	4.10	3.80	3.80	3.50	2.20	2.50	2.30	2.60
Domain 3	$\ln(P/P_0)$	−4.91	−4.88	−4.88	−4.93	−4.96	−4.99	−4.92	−4.98	−4.97	−5.07
	V_m	5.47	3.22	4.15	6.68	5.41	6.50	3.63	3.59	2.80	4.00
	r	2.70	2.60	2.75	2.90	3.00	3.00	3.00	3.20	3.25	3.40
Domain 4	$\ln(P/P_0)$	−3.01	−3.23	−3.10	−2.90	−3.14	−3.06	−3.08	−3.00	−3.09	−3.39
	V_m	5.92	1.90	3.49	5.39	4.60	4.63	3.80	2.78	3.08	3.18
	r	1.90	1.90	1.90	1.90	1.90	1.90	1.90	1.90	1.90	1.90

Units of V_m: cm^3 g^{-1}

$\ln(P/P_0)$ values at approximately −7.0 kT is present in all samples, its definition decreasing with increasing layer charge. (3) A high-energy domain (domain 1 in Table 2) is present for layer charges $\leqslant 1.20$ at $\ln(P/P_0)$ values of approximately −10.5 kT. It then disappears for higher layer charges. (4) A low-energy domain (domain 4 in Table 2) roughly constant in width and position ($\ln(P/P_0) \approx -3.0$ kT) is present for all the samples.

Figure 5 shows the derivative N_2 adsorption isotherms of the ten saponite samples together with their decomposition obtained from the DIS procedure whereas Table 3 presents the parameters corresponding to the various domains obtained from the decomposition. The shapes of the N_2 derivative adsorption isotherms are very different from those observed when Ar is used as an adsorbate. Such behaviour has been observed for numerous mineral systems such as calcite, apatite (Villiéras *et al.*, 1999), illite (Bardot *et al.*, 1998, 2000) and Al-intercalated saponites (Michot *et al.*, 1998).

Except for the sample with a layer charge of 0.80, these curves exhibit common features. (1) A broad high-energy peak centred on $\ln(P/P_0)$ values of −13 kT is present for all samples. It is modelled using either two or three peaks in the decomposition procedure (domains 1 to 3 in Table 3). (2) A broad medium-energy peak is located at $\ln(P/P_0)$ values of approximately −9 kT (domain 4 in Table 3). (3) A peak located at $\ln(P/P_0)$ values of approximately −6 kT (domain 5 in Table 3), the

position of which evolves towards higher energy (i.e. lower $\ln(P/P_0)$) with increasing layer charge. (4) A low-energy domain (domain 6 in Table 3) roughly constant in width and position ($\ln(P/P_0) \approx -2.0$ kT) is present for all the samples.

DISCUSSION

As shown in Fig. 6, except for the sample with a layer charge of 0.80, the Ar surface area corresponding to the last three domains matches exactly the non-microporous specific surface area obtained by the t-plot procedure applied to N_2 step-by-step adsorption experiments. This observation suggests three conclusions which are discussed below. (1) For layer charges $\geqslant 1.30$, Ar atoms probe only the geometrical surface area of the samples. (2) For layer charges $\leqslant 1.20$, Ar atoms are sensitive to structural high-energy sites. The amount adsorbed on these sites is lower than the total 'micropore' volume observed using N_2 as the adsorbate. (3) The 'micropores' observed in classical N_2 adsorption-desorption procedures are probably not true geometrical micropores but rather high-energy sites with a structural origin.

Geometrical properties of saponite particles

Based on the surface chemistry of saponite and previous results obtained from kaolinite, talc and illites, it seems logical, when Ar is used as an
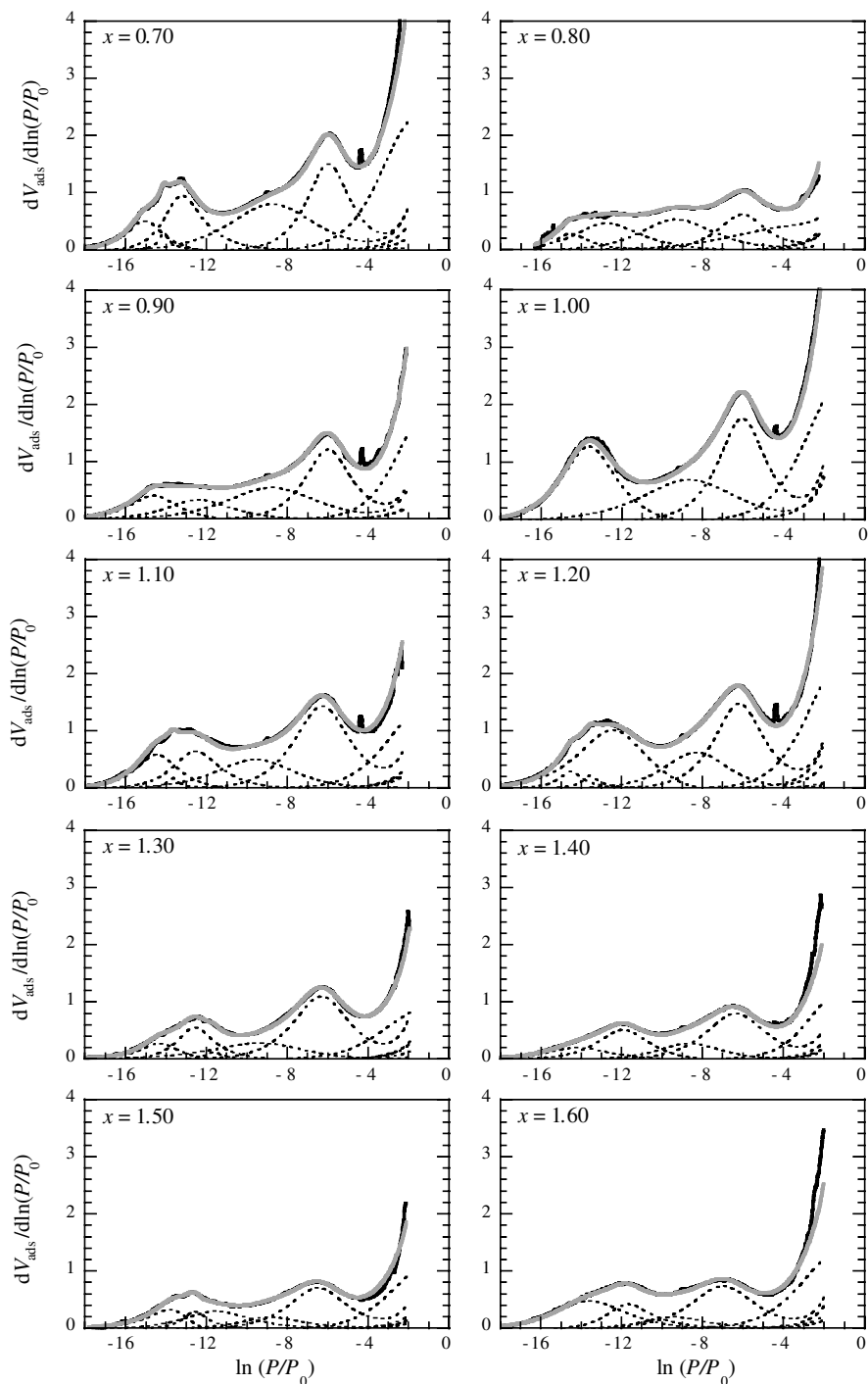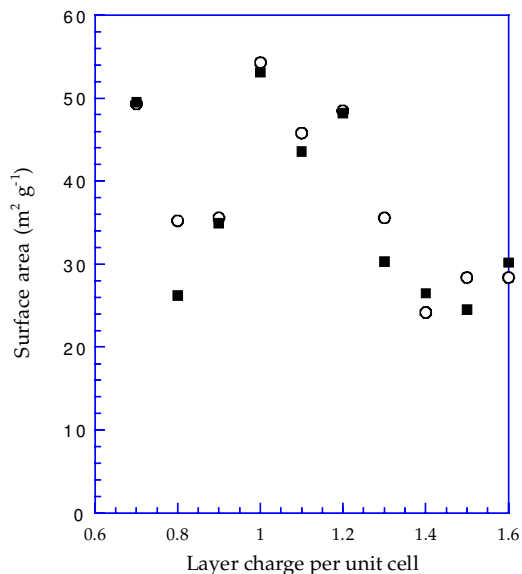
FIG. 5. Derivative N_2 adsorption isotherms obtained at 77 K on synthetic saponites with increasing layer charge together with their decomposition using the Derivative Isotherm Summation (DIS) method. Outgassing conditions: 150°C, 0.001 Pa.

TABLE 3. Main parameters obtained from the application of the DIS method to N_2 adsorption at 77 K on saponites with increasing layer charge. Outgassing conditions: 150°C, 0.001 Pa.

Layer charge per unit cell		0.70	0.80	0.90	1.00	1.10	1.20	1.30	1.40	1.50	1.60
Domain 1	$\ln(P/P_0)$	−15.04	−14.52	−14.61	—	−14.46	−14.52	−14.31	−14.19	−13.80	−13.60
	V_m	1.21	0.63	1.24	—	1.63	0.49	0.68	0.77	0.83	2.13
	r	2.70	5.00	2.80	—	3.00	3.50	2.50	3.00	1.80	3.50
Domain 2	$\ln(P/P_0)$	−14.10	—	—	−13.63	−13.65	−13.56	−12.57	—	−12.57	—
	V_m	0.27	—	—	4.40	0.16	0.27	1.34	—	0.50	—
	r	5.00	—	—	3.10	4.50	4.00	3.90	—	3.90	—
Domain 3	$\ln(P/P_0)$	−13.20	−12.75	−12.42	—	−12.54	−12.45	−11.64	−11.93	−11.55	−11.70
	V_m	2.51	1.94	1.35	—	1.96	4.27	0.15	1.66	1.24	1.26
	r	5.5	4.00	3.60	—	3.80	2.60	5.00	3.00	4.00	6.00
Domain 4	$\ln(P/P_0)$	−8.73	−9.30	−8.77	−8.65	−9.57	−8.31	−9.36	−8.65	−8.82	−9.45
	V_m	4.21	2.44	3.03	3.99	2.40	2.43	1.55	1.02	0.76	0.79
	r	3.10	3.60	3.00	2.90	2.90	3.00	2.50	3.30	3.80	4.00
Domain 5	$\ln(P/P_0)$	−5.96	−6.03	−5.97	−6.04	−6.27	−6.18	−6.30	−6.36	−6.48	−6.99
	V_m	4.20	1.87	3.62	5.37	5.01	4.71	3.87	2.94	2.55	2.96
	r	3.00	2.90	2.90	2.90	2.80	2.90	2.80	2.90	2.85	2.90
Domain 6	$\ln(P/P_0)$	−2.07	−3.75	−2.46	−2.24	−2.40	−2.10	−2.28	−1.74	−2.28	−2.16
	V_m	4.42	2.12	2.44	3.84	2.44	3.35	1.61	1.62	1.73	2.38
	r	1.90	1.90	1.90	1.90	1.90	1.90	1.90	1.90	1.80	1.80

Units of V_m: cm^3 g^{-1}

FIG. 6. Comparison between the geometrical surface areas obtained for synthetic saponites with increasing layer charge from the N_2 t-plot (empty circles) and from the DIS procedure applied to derivative Ar adsorption isotherms (filled squares).

adsorbate, to assign domain 2 to the adsorption of Ar atoms on the edge faces of saponite and domains 3 and 4 to the adsorption on basal faces, which allows us to define a lamellarity index I_L as:

$$I_L = \frac{\text{Surface area of basal faces}}{\text{Total geometrical surface area}}$$

Apart from the sample with a layer charge of 0.80 where the quantity of lateral faces is abnormally high, I_L is ~85% for samples with layer charges $\leqslant 1.20$ and ~88% for samples with layer charges $\geqslant 1.30$ (Table 4). To illustrate the changes occurring in particle shape, the particles were modelled as perfect monodisperse regular hexagons. In this case, surface areas of basal and lateral faces can be used simply to derive the thickness and length of the particles (Table 4). Figure 7 shows the evolution of both parameters as a function of layer charge. The thickness remains roughly constant while the length is multiplied by more than two when the layer charge reaches 1.30. For this layer charge, each ditrigonal ring formed by the arrangement of tetrahedra contains at least one Al atom which shows the influence of Al density on crystal growth.

TABLE 4. Geometrical and structural parameters deduced from the application of the DIS method to Ar adsorption at 77 K on saponites with increasing layer charge.

| Layer charge per unit cell	0.70	0.80	0.90	1.00	1.10	1.20	1.30	1.40	1.50	1.60
Basal surface area (m² g⁻¹)	42.3	19.0	28.3	44.8	37.1	41.3	27.6	23.6	21.8	26.6
Edge surface area (m² g⁻¹)	7.27	7.20	6.60	8.27	6.46	6.86	2.78	2.86	2.71	3.64
Lamellarity index (%)	85.3	72.5	81.9	84.4	85.2	85.7	89.2	89.0	88.0	86.8
Length (nm)	235.3	237.6	259.2	206.9	264.8	249.4	615.4	598.2	631.3	470.0
Thickness (nm)	17.5	39.0	26.2	16.5	20.0	17.9	26.8	31.4	34.0	27.8
V_{ads} on high-energy sites (cm³ g⁻¹)	2.30	1.34	1.09	1.36	1.03	0.67	0	0	0	0
Ar molecules on high-energy sites	6.2×10^{19}	3.6×10^{19}	2.9×10^{19}	3.7×10^{19}	2.7×10^{19}	1.8×10^{19}	0	0	0	0
Number of ditrigonal cavities	1.7×10^{20}	7.8×10^{19}	1.2×10^{20}	1.8×10^{20}	1.5×10^{20}	1.7×10^{20}	1.1×10^{20}	9.7×10^{19}	8.9×10^{19}	1.1×10^{20}
Number of talc-like ditrigonal cavities	8.2×10^{19}	3.1×10^{19}	3.8×10^{19}	4.6×10^{19}	2.7×10^{19}	1.7×10^{19}	2.8×10^{18}	0	0	0
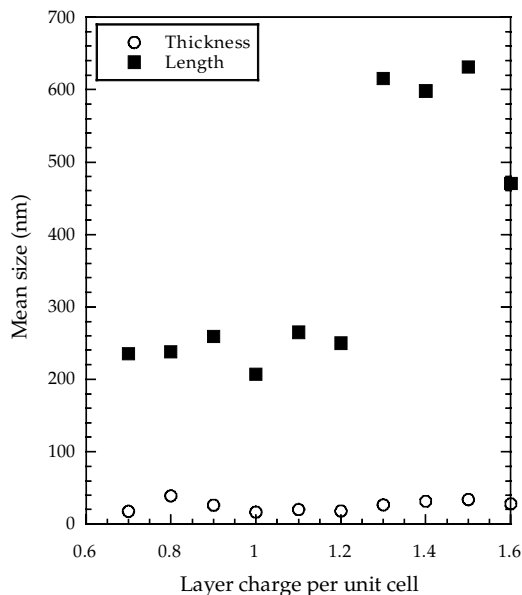
Fig. 7. Evolution with layer charge of the length and thickness of synthetic saponite particles estimated assuming a regular hexagonal shape.

As observed in numerous studies, N_2 derivative adsorption isotherms display more complex shapes and exhibit more high-energy sites than the corresponding Ar isotherms. In contrast to what was observed with Ar, no domain can be clearly assigned to adsorption on the edges. The two lower-energy domains observed can be assigned to the adsorption of nitrogen molecules on the basal planes of saponite. However, the surface area corresponding to these two domains represents between 80 and 90% of the basal surface area measured by Ar adsorption. Such a difference could be assigned to an incorrect choice of the cross-sectional area of Ar atoms but as discussed in the following sections, other explanations linked to specific adsorption sites for N_2 seem more likely.

Ar high-energy sites

Argon derivative adsorption isotherms exhibit high-energy sites only for layer charges $\leqslant 1.20$. Such sites had already been observed for talc (Michot *et al.,* 1994) which is the uncharged end-member of the saponite series. In that case, high-energy sites could be assigned unambiguously to OH groups located at the bottom of the uncharged

ditrigonal cavities. As mentioned in the previous section, for a layer charge of 1.30, all ditrigonal rings contain one Al atom. The disappearance of high-energy sites then corresponds exactly to the disappearance of 'talc-like' ditrigonal rings on the basal faces of saponite. Using structural data and decomposition results from the DIS procedure, the number of talc-like ditrigonal cavities can be obtained for each sample and compared with the number of Ar atoms adsorbed in high-energy sites (Table 4 and Fig. 8). The size of a ditrigonal cavity was taken as a constant value of 24.5 Å^2 independent of the layer charge, as results obtained by Suquet (1978) show that the b crystallographical parameter is nearly constant for dehydrated synthetic saponites. It appears that both values match very well, thus confirming the assignment of the high-energy sites to the 'talc-like' ditrigonal cavities of the basal faces of saponites. Such strong interaction between OH groups and Ar atoms was observed previously in the case of Al-intercalated saponites where the acidic OH groups of the intercalated Al polycations were the primary adsorption sites for both Ar and N_2 (Michot *et al.,* 1998).

N_2 high energy sites.

In the case of N_2, high-energy sites (domains 1 to 4 in Table 3) are observed whatever the layer charge, and the number of those high-energy sites is always greater than that observed with Ar (even after taking into account the edge faces that are not clearly marked in the case of N_2). Therefore, additional adsorption sites different from 'talc-like' ditrigonal cavities must be considered. The corresponding amount adsorbed will be referred to as V_{HES1} (volume adsorbed on high-energy sites of type 1).

Furthermore, as mentioned previously, the surface area derived from domains 5 and 6 is less than the basal surface area derived from Ar adsorption. In view of the near perfect match observed in Fig. 8, it seems that the Ar values must be valid. This suggests that in the case of N_2, some of the adsorption sites, referred to as V_{HES2}, on the basal faces are located in the higher-energy domain where they are not clearly distinguishable. At present, using gas adsorption results only, the exact assignment of domains 1 to 4 cannot be achieved and site assignments can only be global and based on Ar adsorption results.
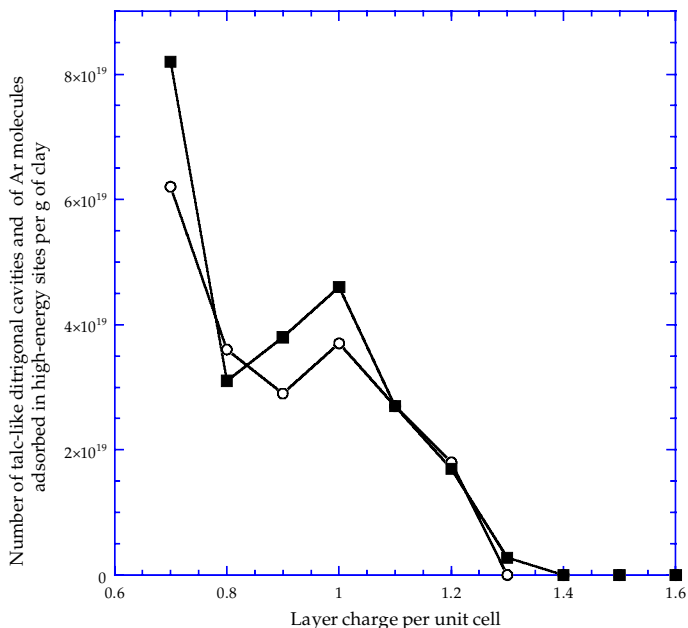
FIG. 8. Comparison between the number of talc-like ditrigonal cavities (filled squares) and the number of Ar molecules adsorbed on high-energy sites (empty circles) per g of synthetic saponite.

The total amount of high-energy sites for nitrogen V_{HES} can be estimated by using the formula:

$$V_{HES} = V_{tot} - V_5 - V_6 - (S_{edgeAr})/4.37 \quad (10)$$

which can be split into two parts:

$$V_{HES1} = V_{tot} - (S_{edgeAr}+S_{basAr})/4.37 \quad (11)$$
$$V_{HES2} = V_{HES} - V_{HES1} \quad (12)$$

where V_5 and V_6 are the volumes adsorbed on domains 5 and 6 of the DIS decomposition (Table 3), V_{tot} is the total N_2 adsorbed volume and S_{edgeAr} and S_{basAr} are the surface areas of the edge and basal surfaces determined by Ar adsorption.

As shown in Fig. 9, except for the sample with a layer charge of 0.8, V_{HES1} is very close to the number of ditrigonal rings with no Na^+ cations. Indeed, after outgassing under vacuum at 150°C, Na is located in the octahedral cavity directly above the OH group as revealed by IR and Raman experiments (Pelletier *et al.,* submitted). Nitrogen then seems to exhibit a strong affinity for empty cages of the basal planes and N_2 molecules adsorbed in those sites do not modify the amount of basal surface sites available.

Figure 10 compares V_{HES2} with the number of Na^+ cations on the basal faces calculated from the layer charge and the extension of the basal surface area. The two sets of data follow the same pattern but the values are different, the discrepancy increasing with increasing layer charge. Those high-energy sites are therefore probably related to the cations of the basal planes but there is not a 1:1 relationship between N_2 molecules and Na^+ cations. One possible explanation for this behaviour could be found in the arrangement of Na^+ cations on the basal faces between isolated cations (Na_i) and cation doublets, i.e. in two adjacent cages (Na_d). As the statistical determination of the various configurations is not straightforward, we simulated the arrangement of Na^+ ions on the basal surfaces (consisting of 1133 ditrigonal rings) by first placing the Al for Si substitution. The program used an exclusion rule, i.e. for layer charges $\leqslant 1.33$, no ditrigonal ring contains two Al atoms. The Na^+ ions were then placed randomly in one of the three ditrigonal cages adjacent to the substitution. The simulation was run 100 times for each layer charge and the average number of Na doublets was then determined. Figure 11 compares V_{HES2} with Na_i, Na_d as well as $Na_i + Na_d$. It appears that the best
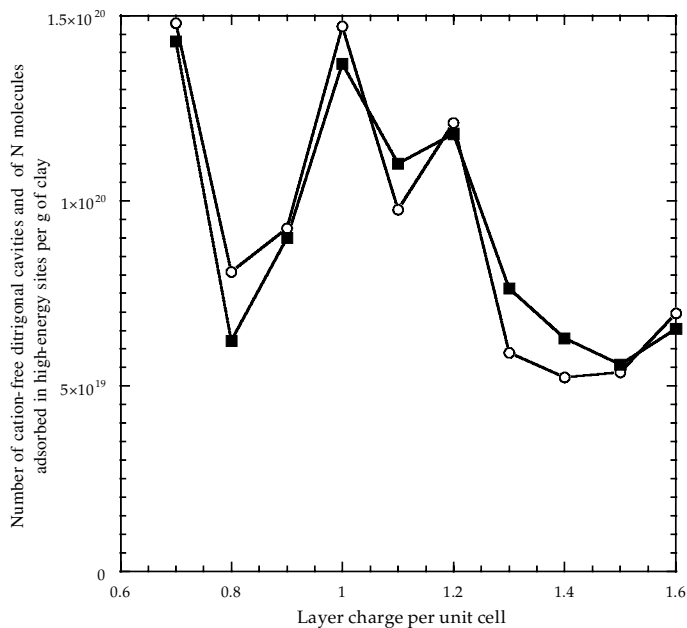
FIG. 9. Comparison between the number of cation-free ditrigonal cavities (filled squares) and the number of N_2 molecules adsorbed on high-energy sites of type 1 (empty circles) per g of synthetic saponite.
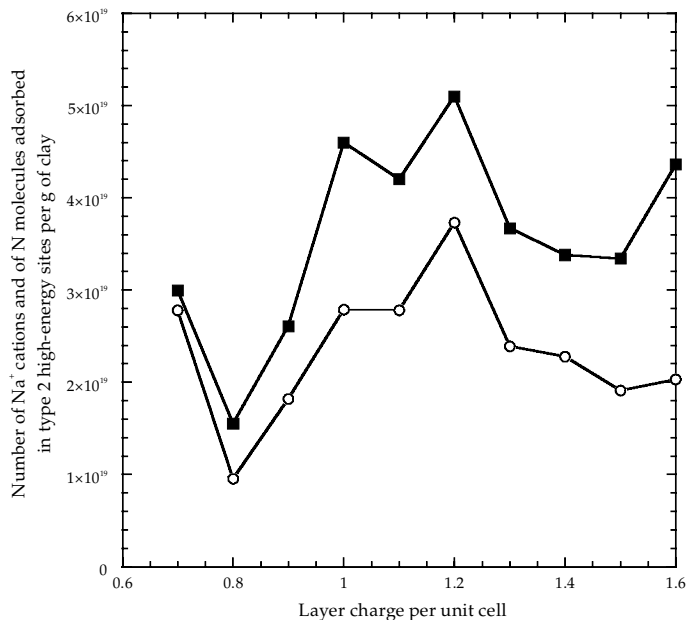

FIG. 10. Comparison between the number of cations (filled squares) and the number of N_2 molecules adsorbed on high-energy sites of type 2 (empty circles) per g of synthetic saponite.
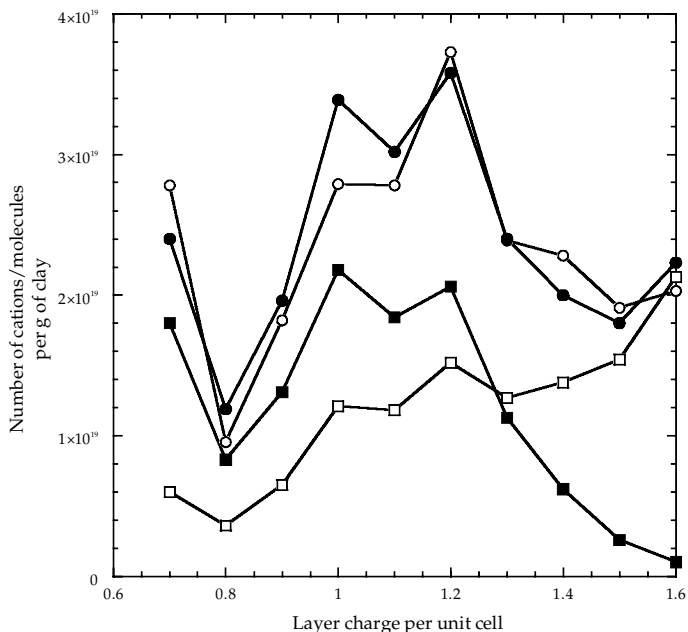
FIG. 11. Comparison between the number of isolated cations (filled squares), the number of cation doublets (empty squares), the sum of isolated cations and doublets (filled circles) and the number of N_2 molecules adsorbed on high-energy sites of type 2 (empty circles) per g of synthetic saponite.

match is obverved when considering $Na_i + Na_d$ which suggests that, in the case of a doublet, one N_2 molecule interacts with both Na^+ ions.

As a summary, three types of high-energy sites for N_2 are present on the basal faces of saponites: empty ditrigonal cavities, isolated Na, and Na doublets.

Adsorption mechanisms

Taking into account all the information obtained for Ar and N_2, it is possible to propose a schematic sequence for the adsorption of both molecules on the basal planes of saponites (Figs 12–14).

As already demonstrated, for layer charges <1.30, Ar atoms adsorb first on the OH groups of the talc-like ditrigonal cavities (Fig. 12b). The next basal Ar adsorption sites correspond to the main adsorption peak located around $-5 kT$ on the derivative isotherm (Table 2). Recent high-resolution gas adsorption measurements on illite samples exchanged with different cations revealed that the position of the main Ar adsorption peak depends linearly on the electronegativity of the exchangeable cation (Bardot, 1998). With increasing layer charge, the main adsorption peak for saponite is

located at a constant energy but with a lesser dispersion of adsorption energies as revealed by its sharpening as a function of layer charge (Table 2). As values of the Lennard-Jones potential (Gerschel, 1995) reveal that Ar is more attracted by the O atoms of the siloxane surface than by the compensating cations, the effect of the cation must be indirect. The most favourable adsorption sites may then be the O triads located in the vicinity of a compensating cation (Fig. 12c). For small layer charges, the basal planes are formed of such sites as well as of O triads located further away from Na^+ cations. This provokes a widening of the energy distribution noticeable by a rather broad peak on the derivative adsorption isotherm. After the filling of these adsorption sites, monolayer completion would then be driven mainly by lateral interactions between adsorbing and adsorbed Ar atoms.

For layer charges $\geqslant 1.30$, the talc-like cavities do not exist anymore, which explains the disappearance of high-energy sites. Assuming the same structuring effects of the cations, it appears (Fig. 13b) that nearly all adsorption sites will be situated in the vicinity of a cation which accounts for the smaller degree of energy dispersion observed for Ar adsorption on the basal planes.
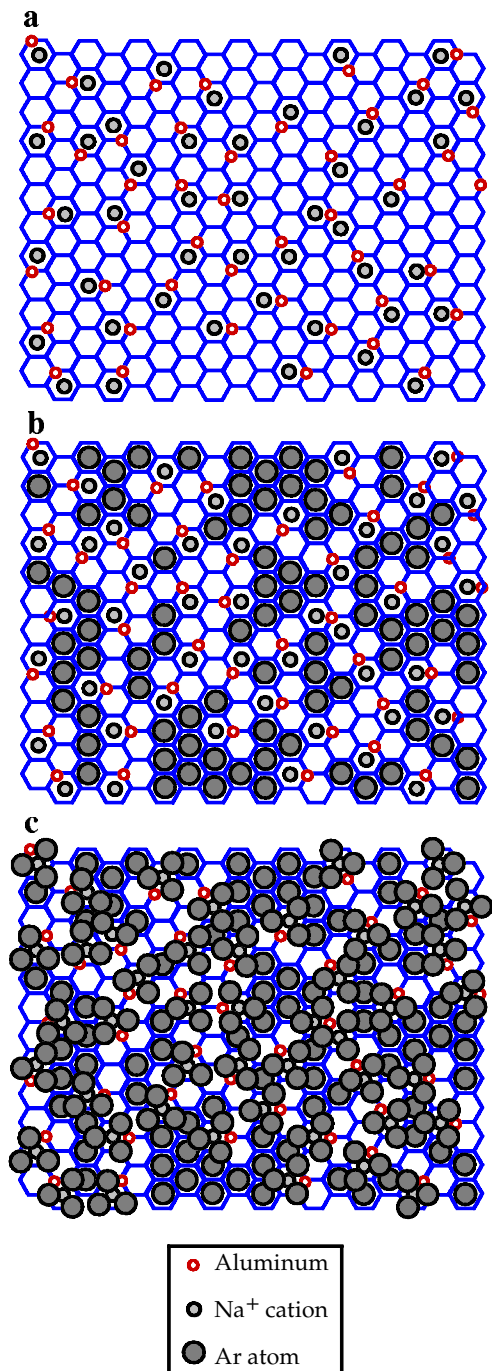
FIG. 12. Schematic representation of the different steps which occur upon adsorption of Ar molecules onto the basal planes of synthetic saponite with a layer charge of 0.90 per unit cell.
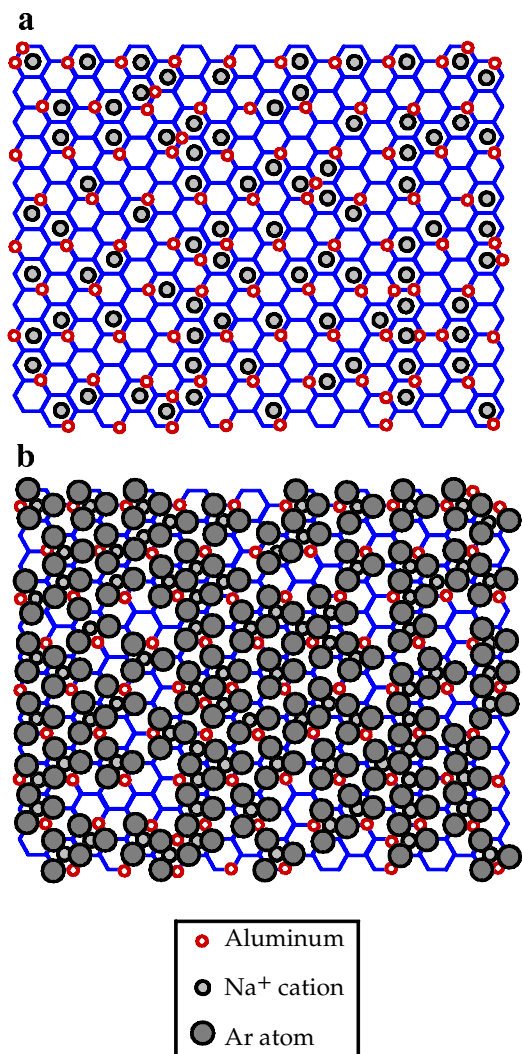

FIG. 13. Schematic representation of the different steps which occur upon adsorption of Ar molecules onto the basal planes of synthetic saponite with a layer charge of 1.50 per unit cell..

As in the previous case, monolayer formation is thereafter mainly driven by lateral interactions between Ar atoms.

In the case of N_2, the primary adsorption sites are likely to be the empty ditrigonal rings (Fig. 14b). The resolution of the decomposition does not allow us to distinguish between the talc-like and other empty ditrigonal cavities. Subsequent N_2 molecules adsorb on the edge faces and close to the cations,

a

b

c
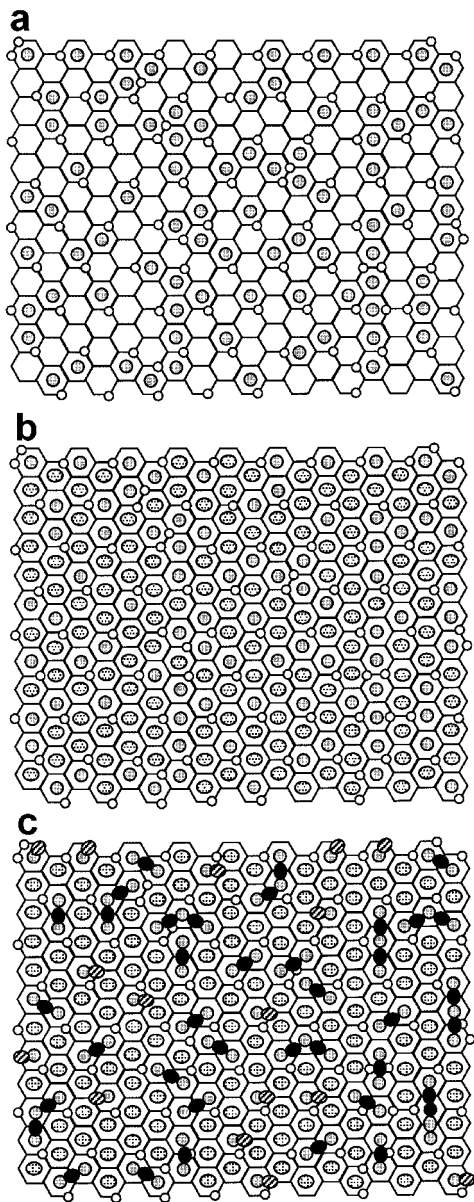
○	Aluminium
◉	Na+ cation
⊕	N2 adsorbed in empty cages
⊘	N2 adsorbed close to one Na+ cation
●	N2 adsorbed close to two Na+ cations

with no possible distinction between those two types of sites. Adsorption finally proceeds on the remaining space of the basal faces, probably close to the exchangeable cations in the first instance, as this occurs with a shift towards higher energy. Final monolayer completion would then be driven mainly by lateral interactions between adsorbing and adsorbed N_2 molecules as already suggested in the case of Ar adsorption.

SUMMARY AND CONCLUSIONS

High-resolution gas adsorption appears to be a viable tool for studying the surface organization of clay minerals. Using series of well characterized samples, where one structural parameter (layer charge in the present case) varies in a systematic way, complex adsorption features can be understood.

In the case of clay minerals, classical N_2 adsorption methods used for the determination of specific surface areas and micropore volumes (Rutherford *et al.*, 1997; Altin *et al.*, 1999; Lee *et al.*, 1999) do not yield true geometric data because of the presence of high-energy sites that are generally wrongly assigned to micropores.

Argon adsorption is much more suitable than N_2 adsorption for unravelling the geometrical features of clay particles. Indeed, for all the Na-saponite samples studied, whatever the charge, the aspect ratio of the particles can be obtained from the decomposition of the derivative adsorption isotherms after taking into account the presence, for low-charge samples, of high-energy sites corresponding to the talc-like ditrigonal cavities of the basal surfaces. Argon atoms do not exhibit any specific interactions with the compensating Na^+ cations but the presence of these ions on the basal surfaces seems to influence the organization of the adsorbed monolayer. Structural experiments such as neutron diffraction near monolayer completion should then be carried out for a better characterization of the adsorbed layers.

When N_2 is used as an adsorbate, the distinction between edge and basal faces is much less clear, which precludes the use of this adsorbate in the definition of the aspect ratio of clay platelets. Nitrogen molecules interact strongly with all the

FIG. 14. Schematic representation of the different steps which occur upon adsorption of N_2 molecules onto the basal planes of synthetic saponite with a layer charge of 1.40 per unit cell.

cation-free ditrigonal cavities on the basal faces of Na-saponite. In contrast with Ar, N_2 molecules appear to be sensitive to surface Na^+ cations, whose arrangement on the surface would then control the organization of adsorbed N_2 molecules. It would be very useful to combine this gas adsorption approach with spectroscopic measurements such as neutron diffraction or low-temperature Raman spectroscopy experiments.

REFERENCES

Altin O., Ozbelge H.O. & Dogu T. (1999) Effect of pH in an aqueous medium on the surface area, pore size distribution, density and porosity of montmorillonite. *Journal of Colloid and Interface Science,* **217,** 19−27.

Bardot F. (1998) *Les minéraux argileux et leur hétérogénéité superficielle: Influence de la nature des cations compensateurs de l'illite sur les mécanismes d'adsorption de gaz.* Doc. Sci. Thesis, Institut National Polytechnique de Lorraine, Nancy, France.

Bardot F., Villiéras F., Michot L.J., François M., Gérard G. & Cases J.M. (1998) High resolution gas adsorption study on illites permuted with various cations: assessment of surface energetic properties. *Journal of Dispersion Science and Technology,* **19,** 739−759.

Bardot F., Villiéras F., Michot L.J., François M., Gérard G. & Cases J.M. (2000) Application of very low relative pressure adsorption volumetry to study surface properties of clay minerals. Pp. 339−344 in: *Clays for our Future. Proceedings of the International Clay Conference, Ottawa* (H. Kodama, A. Mermut & J. Torrance, editors). Ottawa, Canada.

Brady P.V., Cygan R.T. & Nagy K.L. (1996) Molecular controls on kaolinite surface charge. *Journal of Colloid Interface Science,* **183,** 356−364.

Braggs B., Fornasiero D., Ralston J. & Smart R.St.C. (1994) The effect of surface modification by an organosilane on the electrochemical properties of kaolinite. *Clays and Clay Minerals,* **42,** 123−136.

Cases J.M., Cunin P., Grillet Y., Poinsignon C. & Yvon J. (1986) Methods of analysing the morphology of kaolinites: relations between crystallographic and morphological properties. *Clay Minerals,* **21,** 55−68.

Conley R.F. & Lloyd M.D. (1971) Adsorption studies on kaolinites. II. Adsorption of amines. *Clays and Clay Minerals,* **19,** 273−282.

De Boer J.H., Lippens B.C., Linsen B.G., Broekhoff J.C.P., Van Den Heuvel A. & Osinga Th.J. (1966) The t−curve of multimolecular N_2 adsorption. *Journal of Colloid and Interface Science,* **21,** 405−414.

De la Calle C. & Suquet H. (1988) Vermiculite. Pp. 455−496 in: *Hydrous Phyllosilicates* (S.W. Bailey, editor). Reviews in Mineralogy, **19.** Mineralogical Society of America, Washington, D.C.

Du Q., Sun Z., Forsling W. & Tang H. (1997) Acid-base properties of aqueous illite surfaces. *Journal of Colloid and Interface Science,* **187,** 221−231.

Eberl D.D., Drits V., Środoń J. & Nüesch R. (1996) *Mudmaster: a program for calculating crystallite size distribution and strain from the shapes of X-ray diffraction peaks.* U.S. Geological Survey Open File Report 96−171.

Gerschel A. (1995) *Liaisons intermoléculaires - Les forces en jeu dans la matière condensée.* InterEditions/CNRS Edition, Paris.

Giese R.F. (1988) Kaolin minerals. Structure and stabilities. Pp. 29−66 in: *Hydrous Phyllosilicates* (S.W. Bailey, editor). Reviews in Mineralogy, **19,** Mineralogical Society of America, Washington D.C.

Hamilton D.L. & Henderson C.M.B. (1968) The preparation of silicate compositions by a gelling method. *Mineralogical Magazine,* **36,** 832−838.

Kronberg B., Kuortti J. & Stenius P. (1986) Competitive and cooperative adsorption of polymers and surfactant on kaolinite surfaces. *Colloids and Surfaces,* **18,** 411−425.

Kulik D.A., Aja S.U., Sinitsyn V.A. & Wood W.A. (2000) Acid-base surface chemistry and sorption of some lanthanides on K^+-saturated Marblehead illite: II. A multisite-surface complexation modeling. *Geochimica Cosmochimica Acta,* **64,** 195−213.

Kuwahara Y., Uehara S. & Aoki Y. (1998) Surface microtopography of lath-shaped hydrothermal illite by tapping-mode and contact mode AFM. *Clays and Clay Minerals,* **46,** 574−542.

Lambert J.-F., Chevalier S., Franck R., Suquet H. & Barthomeuf D. (1994) Pillared Al-saponites. Part II, NMR studies. *Journal of Chemical Society, Faraday Transactions,* **90,** 675−680.

Lee J.-F., Lee C.-K. & Juang L.-C. (1999) Size effect of exchange cation on the pore structure and surface fractality of montmorillonite *Journal of Colloid and Interface Science,* **217,** 172−176.

Liétard O., Yvon J., Delon J.F., Mercier R. & Cases J.M. (1980) Determination of the basal and lateral surfaces of kaolins. Variation with types of crystalline defects. Pp. 558−582 in: *Fine Particle Processing, Vol. I* (P. Somasundaran, editor).

AIME, New York.

Ma C. & Eggleton R.A. (1999) Cation exchange capacity of kaolinite. *Clays and Clay Minerals,* **47**, 174−180.

Michot L., François M. & Cases J.M. (1990) Surface heterogeneity studied by a quasi-equilibrium adsorption procedure. *Langmuir,* **6**, 637−643.

Michot L., Villiéras F., Yvon J. & Fourty G. (1993) Multistage wet grinding of talc. Relation between physico-chemical parameters of the filler and mechanical properties of filled polypropylenes. *Journal of Material Science,* **28**, 1856−1866.

Michot L.J., Villiéras F., François M., Yvon J., Le Dred R. & Cases J.M. (1994) The structural microscopic hydrophilicity of talc. *Langmuir,* **10**, 3765−3773.

Michot L.J., Villiéras F., Lambert J.F., Bergaoui L., Grillet Y. & Robert J.L. (1998) Surface heterogeneity in micropores of pillared clays: the limits of classical pore-filling mechanisms. *Journal of Physical Chemistry B,* **102 (18)**, 3466−3476.

Mühlenweg H. & Dan Hirleman E. (1998) Laser diffraction spectroscopy: influence of particle shape and shape adaptation technique. *Particle and Particle Systems Characterization,* **15**, 163−169.

Nagy K.L. & Blum A.E. (1994) *Scanning Probe Microscopy of Clay Minerals*. CMS Workshop lectures, Vol. 7. The Clay Minerals Society, Boulder, CO.

Pelletier M., Michot L.J., Barrès O., Humbert B. & Robert J.L. (submitted) Influence of layer charge on the hydroxyl stretching of trioctahedral clay minerals: an Infrared and Raman study of synthetic Na and K-saponites. *American Mineralogist*.

Poirier J.E. & Cases J.M. (1991) Anionic surfactant adsorption onto silicate minerals: the role of the cations. *Colloids and Surfaces,* **55**, 333−344.

Psyrillos A., Howe J.H., Manning D.A.C. & Burley S.D. (1999) Geological controls on kaolin particle shape and consequences for mineral processing. *Clay Minerals,* **34**, 193−208.

Rémy J.C. & Orsini L. (1976) Utilisation du chlorure de cobaltihexamine pour la détermination simultanée de la capacité d'échange et des bases échangeables dans les sols. *Science du Sol,* **4**, 269−275.

Rutherford D.W., Chiou C.T. & Eberl D.D. (1997) Effects of exchanged cation on the microporosity of montmorillonite. *Clays and Clay Minerals,* **45**, 534−543.

Sánchez-Soto P.J., Wiewióra A., Avilés M.A., Justo A., Pérez-Maqueda L.A., Pérez-Rodríguez J.L. & Bylina P. (1997) Talc from puebla de Lillo. II. Effect of dry grinding on particle size and shape. *Applied Clay Science,* **12**, 297−312.

Sondi I., Milat O. & Pravdic V. (1997) Electrokinetic potentials of clay surfaces modified by polymers. *Journal of Colloid and Interface Science,* **189**, 66−73.

Środoń J. & Elsass F. (1994) Effect of shape of fundamental particles on XRD characteristics of illite minerals. *European Journal of Mineralogy,* **6**, 113−122.

Šucha V., Środoń J., Elsass F. & McHardy W.J. (1996) Particle shape versus coherent scattering domain of illite/smectite: evidence from HRTEM of Dolna Ves Clays. *Clays and Clay Minerals,* **44**, 665−671.

Suquet H. (1978) *Propriétés de gonflement et structure de la saponite. Comparaison avec la vermiculite.* Doc. ès Sci. Thesis, Univ. Paris VI, France.

Thomas F., Michot L.J., Vantelon D., Montargès E., Prélot B., Cruchaudet M. & Delon J.F. (1999) Layer charge and electrophoretic mobility of smectites. *Colloids and Surfaces A,* **159(2−3)**, 351−358.

Thompson D.W., Macmillan J.J. & Wyatt D.A. (1981) Electron microscope studies of the surface microstructures of layer-lattice silicates. *Journal of Colloid Interface Science,* **82**, 362−372.

Villiéras F., Cases J.M., François M., Michot L.J. & Thomas F. (1992) Textural properties and surface energetic heterogeneity of solids from modelling of low pressure gas adsorption isotherms. *Langmuir,* **8,** 1789−1795

Villiéras F., Michot L.J., Bardot F., Cases J.M., François M. & Rudzinski W. (1997a) An improved derivative isotherm summation method to study surface heterogeneity of clay minerals. *Langmuir,* **13,** 1104−1117.

Villiéras F., Michot L.J., Cases J. M., Berend I., Bardot F., François M., Gérard G. & Yvon J. (1997b) Static and dynamic studies of the energetic surface heterogeneity of clay minerals. Pp. 573−623 in: *Equilibria and Dynamics of Gas Adsorption on Heterogeneous Solid Surfaces* (W. Rudzinski, W.A. Steele & G. Zgrablich, editors). Studies in Surface Science and Catalysis, **104**. Elsevier Science B.V., Amsterdam, The Netherlands.

Villiéras F., Michot L.J., Bernardy E., Chamerois M., Legens C., Gérard G. & Cases J.M. (1999) High resolution gas adsorption study on mineral surfaces: assessment of surface heterogeneity of calcite and apatite. *Colloids and Surfaces A,* **146,** 163−174.

Ward D.B. & Brady P.V. (1998) Effect of Al and organic acids on the surface chemistry of kaolinite. *Clays and Clay Minerals,* **46**, 453−465.

Zbik M. & Smart R.St.C (1998) Nanomorphology of kaolinites: comparative SEM and AFM studies. *Clays and Clay Minerals,* **46**, 153−160.

Zbik M. & Smart R.St.C. (1999) Atomic force microscopy in the estimation of aspect ratio of colloidal kaolinite. Pp. 361−366 in: *Clays for our Future. Proceedings of the International Clay Conference, Ottawa* (H. Kodama, A. Mermut & J. Torrance, editors) Ottawa, Canada.

Zhang Z.Z. & Bailey G.W. (1998) Reactivity of basal surfaces, steps and edges of muscovite: an AFM study. *Clays and Clay Minerals,* **46**, 290−300.